Supplement of Atmos. Chem. Phys., 20, 13905–13927, 2020
https://doi.org/10.5194/acp-20-13905-2020-supplement

Atmospheric Chemistry and Physics
Open Access

Supplement of

Biomass burning events measured by lidars in EARLINET – Part 1: Data analysis methodology

Mariana Adam et al.

Correspondence to: Mariana Adam (mariana.adam@inoe.ro)

S1 List of acronyms

Table S1. List of acronyms

Nomenclature	Definition
ACTRIS	Aerosol, Clouds and Trace Gases Research Infrastructure
a.g.l.	Above ground level
a.s.l.	Above sea level
“atz”, “brc”, “cog”, “ino”, “cbw”, “evo”, “gra”, “lei”, “mas”, “hpb”, “pot”, “sof”, “the”, “waw”	Athens, Barcelona, Belsk, Bucharest, Cabauw, Evora, Granada, Leipzig, Minsk, Observatory Hohenpeißenberg, Potenza, Sofia, Thessaloniki and Warsaw (lidar stations considered in this study).
BAE	Backscatter Ångström exponent. BAE@355/532=-log(βp355/βp532)/log(355/532), BAE@532/1064=-log(βp532/βp1064)/log(532/1064)
BB	Biomass burning
β_p	Particle backscatter coefficient [1/m/sr]
CR(s)	Colour ratio(s). CR_{LR}=LR@532/LR@355, CR_{BAE}=BAE@532/1064/BAE@355/532, CR_{PDR}=PDR@532/PDR@355
EAE	Extinction Ångström exponent. EAE@355/532=-log(κp355/κp532)/log(355/532)
EARLINET	European Aerosol Research Lidar Network
EU, AF, NA, AS	Europe, Africa, North America, Asia continental source regions
EUAF, EUNA, EUAS	Europe + Africa, Europe + North America, Europe + Asia continental source regions
FIRMS	Fire Information for Resource Management System
FRP	Fire radiative power
GDAS	Global Data Assimilation System
HYSPLIT	Hybrid Single-Particle Lagrangian Integrated Trajectory model
IP(s)	Intensive parameter(s)
κ_p	Particle extinction coefficient [1/m]
LR	Lidar ratio [sr]. LR@355=κp355/βp355, LR@532=κp532/βp532
LRT	Long range transport
MODIS	Moderate Resolution Imaging Spectroradiometer
PDR	Linear particle depolarization ratio
QC	Quality control
SE, SW, CE and NE	Southeast, Southwest, Central and Northeast Europe (geographical measurement regions)
SNR	Signal to noise ratio
STD	Standard deviation

S2 Summary of metadata

Table S2. Summary of main features used to calculate the backscatter and extinction coefficient, specific for each b-files and e-files. Detection mode: 1 (photon counting), 2 (analog), 3 (analog + photon counting). Evaluation mode: 1 (Klett-Fernald), 2 (Raman), 3 (aerosol backscatter ratio).

	Detection mode (1/2/3)	Evaluation method (1/2/3)	Raw resolution	Shots averaged	Zenith angle
b355	176/153/**590**	**524**/130/257	**most@3.75m and 60m**	**most@1e4**	**most@0°**
e355	**417**/0/107	0/**516**/0	**most@60m**	**most@1e4**	**most@0°**
b532	229/199/**385**	**335**/296/174	**most@3.75m**, then 7.5m, 15m, 60m	**most@1e4**	**most@0°**
e532	**409**/0/94	0/**496**/0	**most@60m**	**most@1e4**	**most@0°**
b1064	222/**608**/0	**683**/139/0	**most@3.75m**, then 15m and 60m	**most@1e4**	**most@0°**

S3 Calculation of the aerosol layers boundaries

The following approach was considered to calculate the boundaries of the aerosol layers. The order of selecting the optical profile to determine the boundaries of the aerosol layers is the following: βp1064, βp532, βp355, κp532, κp355. In other words, when available, use βp1064. When βp1064 is not available, use βp532. If the latter is not available either, use βp355 and so on. Note that for the times when none of the profiles showed a pollution layer, all profiles for that specific time were excluded.

Once the optical profile (including the associated error profile) and the corresponding altitude profile are available, the algorithm developed to determine the aerosol layers boundaries is run. The steps of the algorithm are the following:

- Perform a smoothing of the optical profile. The number of bins used for smoothing depends on the input resolution. Thus, for a resolution of 3.75 m, we applied moving average over 23 bins. For a resolution of 7.5 m, 15 m, 30 m, 60 m, we used 11 bins, 9 bins, 7 bins and 3 bins, respectively. For the particular cases of "ca" and "oh" systems, we applied a number of bins of 15 and 19, respectively (as the signals were very noisy). The corresponding errors were propagated.
- Employ the function *findpeaks* from Matlab (www.mathworks.com, last access 20191126) to find the maxima, with the following options: the minimum distance between peaks is 300 m (*MinPeakDistance*) and the minimum peak height (*MinPeakHeight*) is as follows: 1e-7 for βp1064, 1.5e-7 for βp532, 3e-7 for βp355, 1e-6 for κp532 and 3e-6 for κp355. The value of the minimum distance between peaks was chosen as in Nicolae et al. (2018). If no peaks are found, the routine returns the message no layers with maximum above *MinPeakHeight*.
- Employ the function *findpeaks* to find the minima, with the following option: the minimum distance between peaks is 300 m (*MinPeakDistance*)
- eliminate adjacent maxima if the "prominence width" (https://www.mathworks.com/help/signal/ug/prominence.html, last access 20191126) overpasses the position of the adjacent maxima
- eliminate small maxima / minima peaks which are smaller than 10% of the maximum / minimum peak
- a maximum peak should be bordered by two minima (which defines the layer boundaries); when the first or the last minimum is missing, a criterion is used to add the missing minimum; thus, the minimum is chosen at a location (> 300 m from the first or the last maximum peak) where the optical property has the minimum value

Following the criteria discussed, there can be cases when it is not possible to find any aerosol layer. Consequently, those profiles were dismissed. Additionally, a manual check was performed and for the cases with non-accurate estimation of the boundaries, the boundaries were manually corrected (~ 40 % of the cases) and sometimes, we added layers which had a maximum below the threshold of the minimum peak height. Thus, we cope with a semi-automatic algorithm. Table 3 shows the number of time stamps when it was possible to determine a layer and at least one optical property could be calculated (column 3). Recall that many profiles were dismissed manually through quality check before we apply the algorithm for layer boundary evaluation and this explain most of the "missed" cases (difference between second and third columns). The initial total number of layers, with at least one optical property (column 4) is greater than the time series (column 3) as most of the times we have more than one layer within a profile. The other columns are discussed in the next section. Overall, we were able to determine 1901 layers for 960 time stamps (out of 1138 in total).

Various authors use different criteria to estimate the layer boundaries. In most of the papers examined, the authors do not describe how they determined the boundaries of the layers. However, the boundaries can be easily identified visually (a common practice when investigating one or few cases). In a few studies it is mentioned the gradient method (Giannakaki et al., 2015; Mattis et al., 2008; Ortiz-Amescua et al., 2017; Preißler et al., 2013). When intensive parameters are available (e.g. EAE or LR), one can determine the boundaries based on intensive parameters being nearly constant in the layer (e.g. Samaras et al., 2015) or based on the ratio of elastic to Raman profiles (Vaughan et al., 2018). In situations when a few layers are visible, one can choose them as a single large layer (e.g. Ansmann et al., 2009).

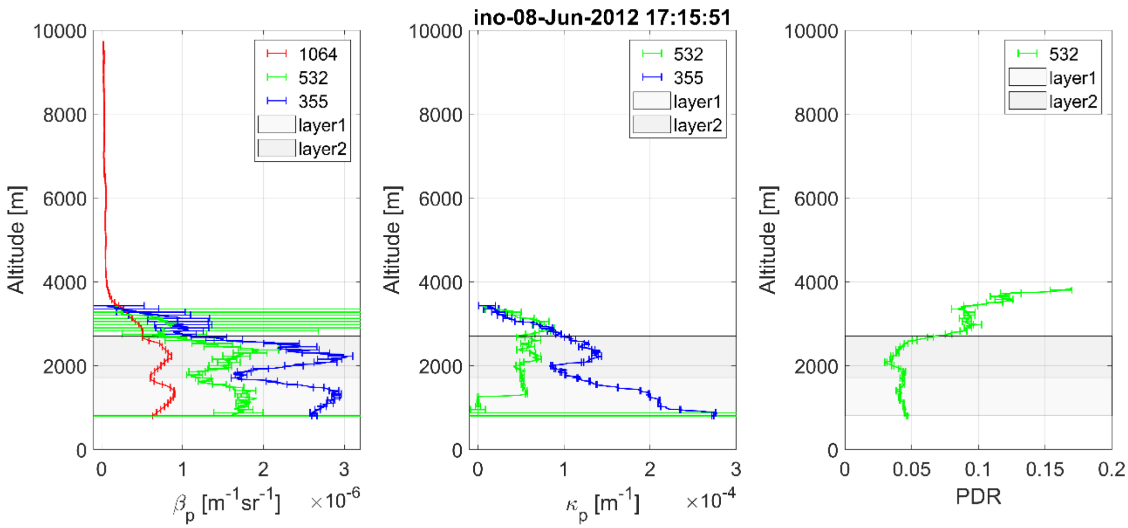

a) Two layers automatically selected based on β_{1064} signal. Layers' boundaries are: [802 1717] m and [1717 2707] m.

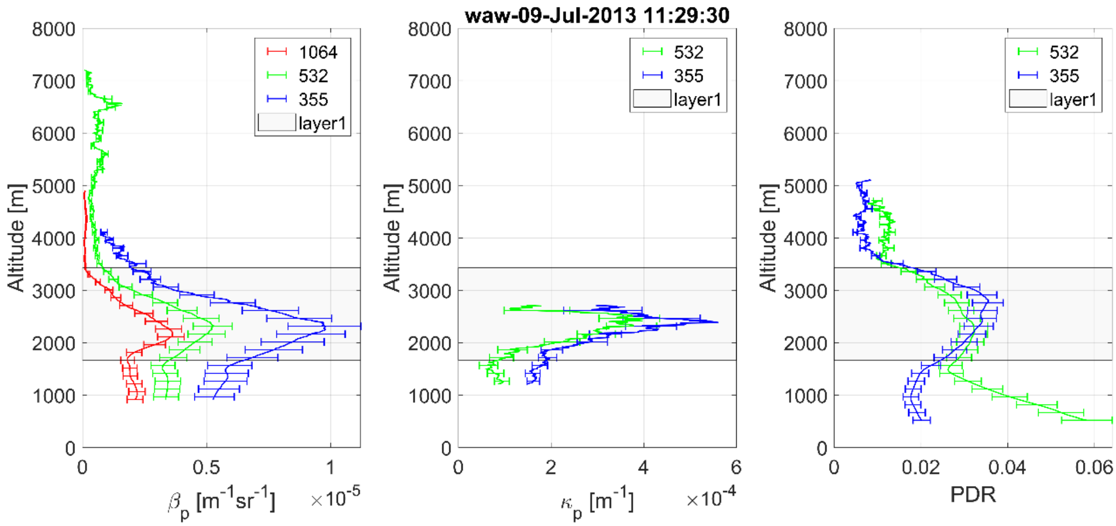

b) One layer automatically selected based on β_{1064} signal. Layer' boundaries are [1670 3426] m.

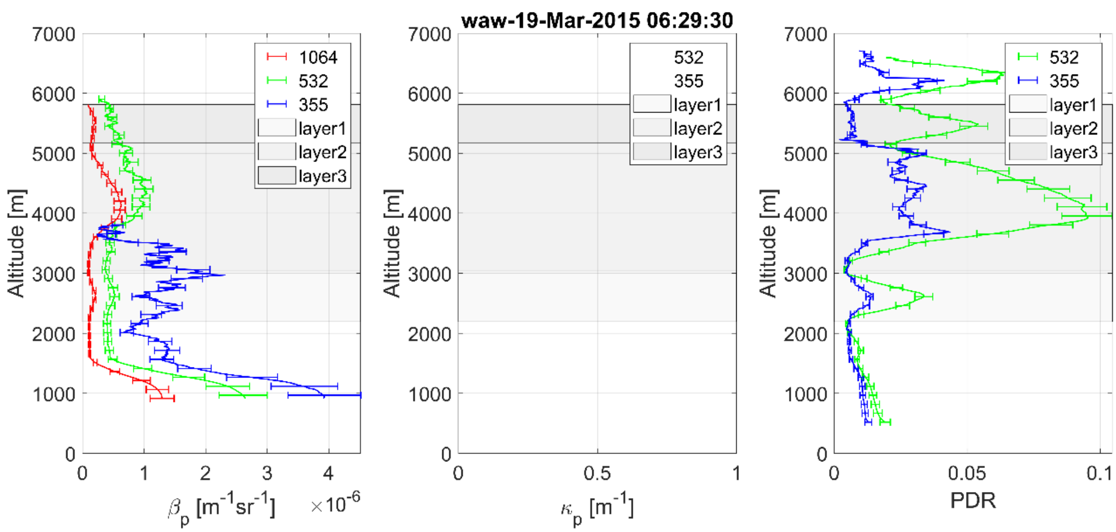

c) Three layers automatically selected based on β_{1064} signal. Layers' boundaries are [2193 3037] m, [3037 5166] m and [5166 5809] m.

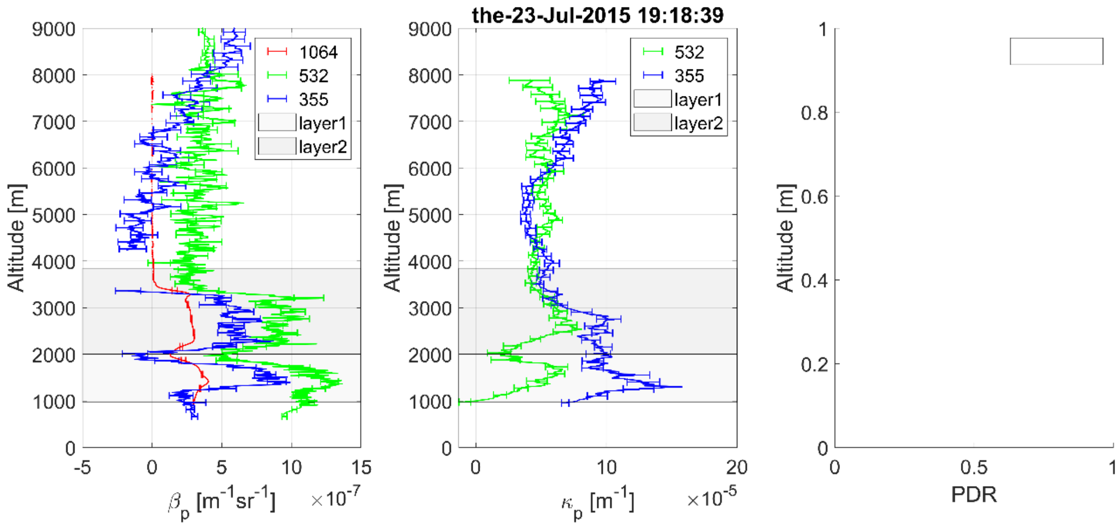

d) Two layers automatically selected based on β_{1064} signal. Layers' boundaries are [968 2002] m and [2002 3847] m.

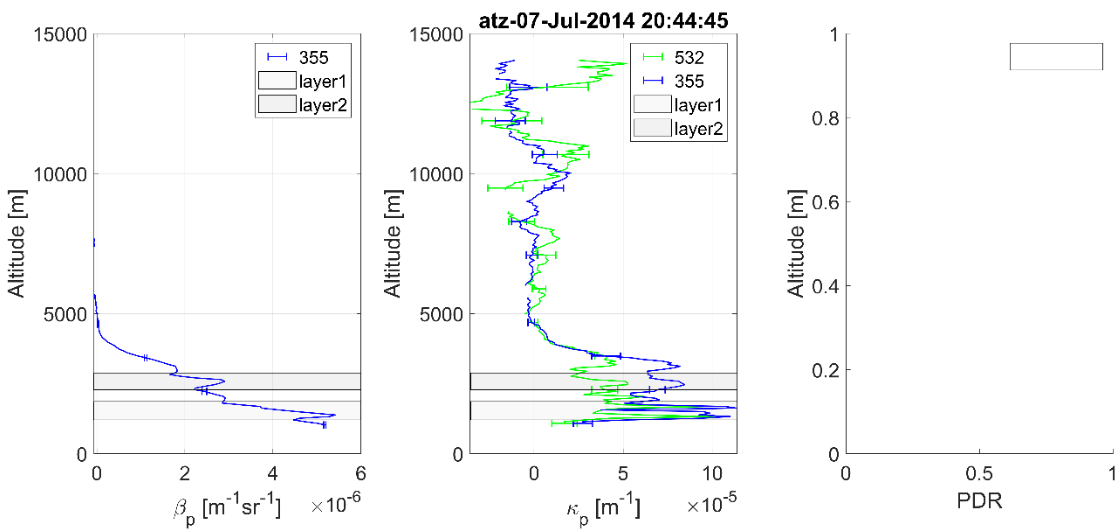

e) Two layers automatically selected, based on β_{355} signal. Layers' boundaries are [1202 1862] m and [2282 2882] m.

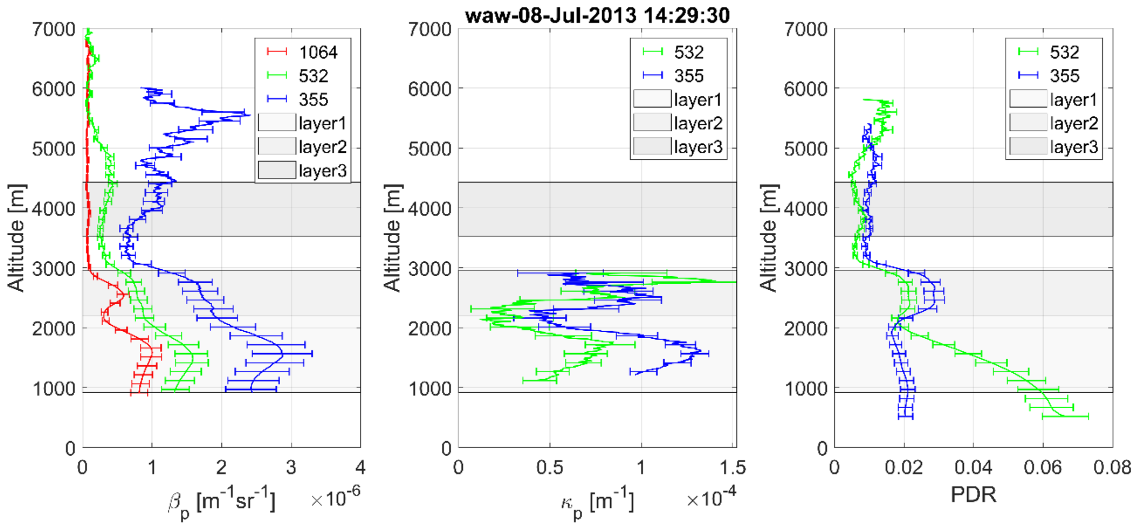

f) Three layers selected based on β_{1064} signal. Layers' boundaries are [915 2193] m, [2193 2962] m and [3530 4427] m. The top of the second layer was manually changed from 3530 m to 2962 m. A fourth layer around 6500m was dismissed.

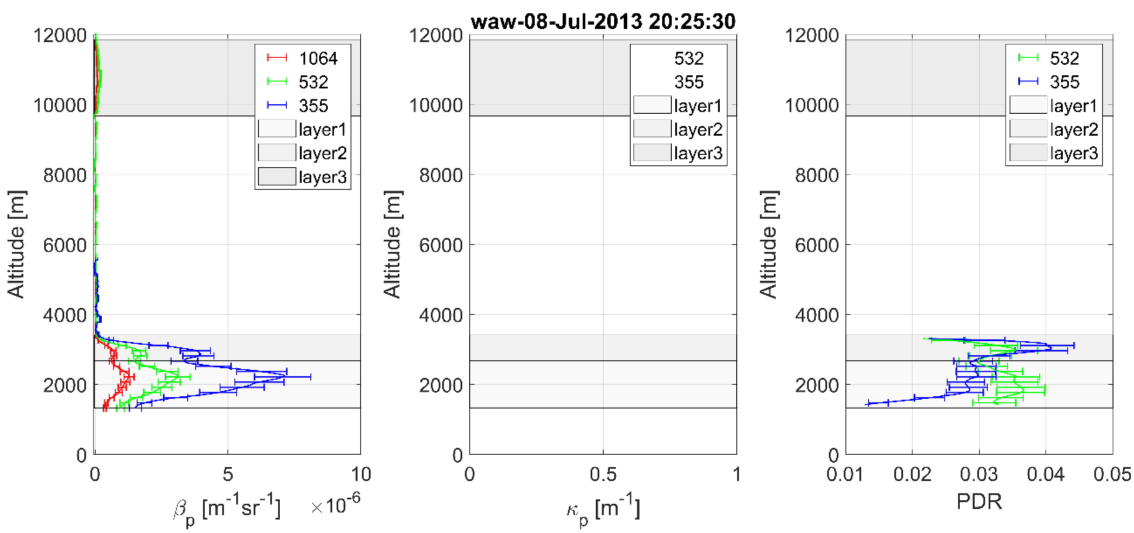

g) Three layers selected based on β_{1064} signal. Layers' boundaries are [1319 2678] m, [2678 3411] m and [9664 11846] m. The third layer was added manually. The top of the second layer was modified from 4061 m to 3411 m.

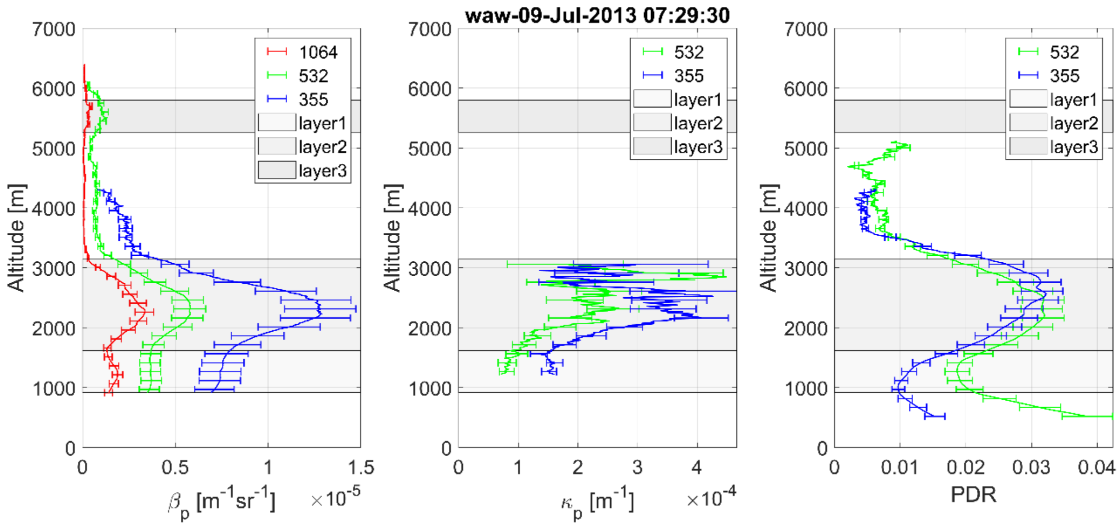

h) Three layers detected based on β_{1064} signal with the boundaries [915 1617] m, [1617 3142] m and [5264 5801] m. The top of the second layer was manually modified from 3612 m to 3142 m.

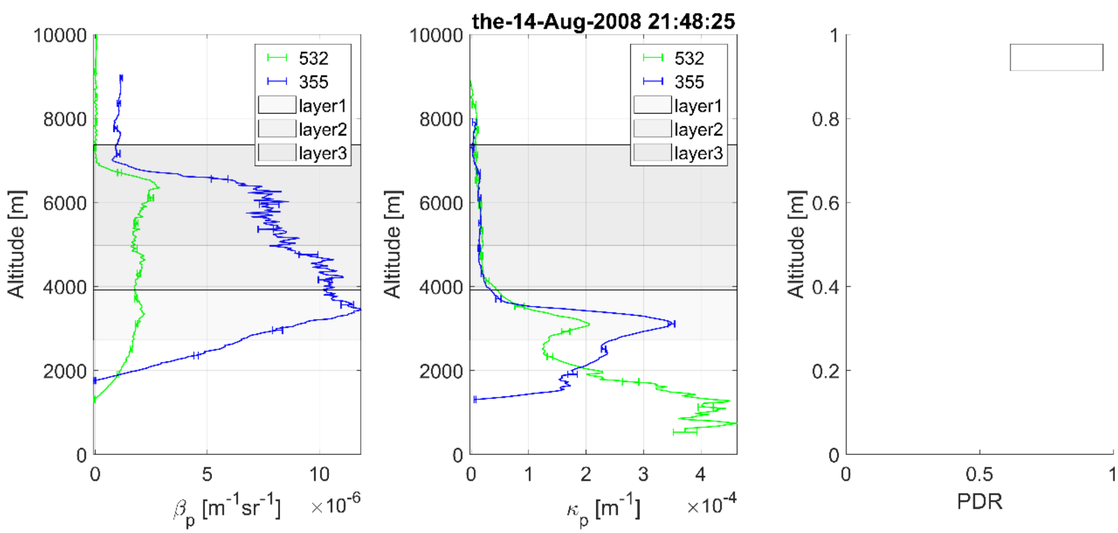

i) Three layers selected, based on β_{532} signal. Layers' boundaries are [2715 3915] m, [3915 4965] m and [4965 7365] m. The bottom of the second and third layers were manually changed from 4485 m to 3915m and from 5295 m to 4965m.

Figure S1. Examples of layers selection, based on β_{1064} signal (a-d, f-h), β_{1532} signal (i) and β_{355} signal (e). Layers are shown by grey areas. All available optical properties are shown (particles backscatter coefficients β_p on the left, particles extinction coefficients κ_p in the middle and particles linear depolarization PDR on the right). The boundaries shown in a-e plots are the automatic output of the algorithm. In the f-i plots, one or more boundaries retrieved by the algorithm were manually adjusted.

S4 Example number of layers selected and corresponding optical parameters available for each layer

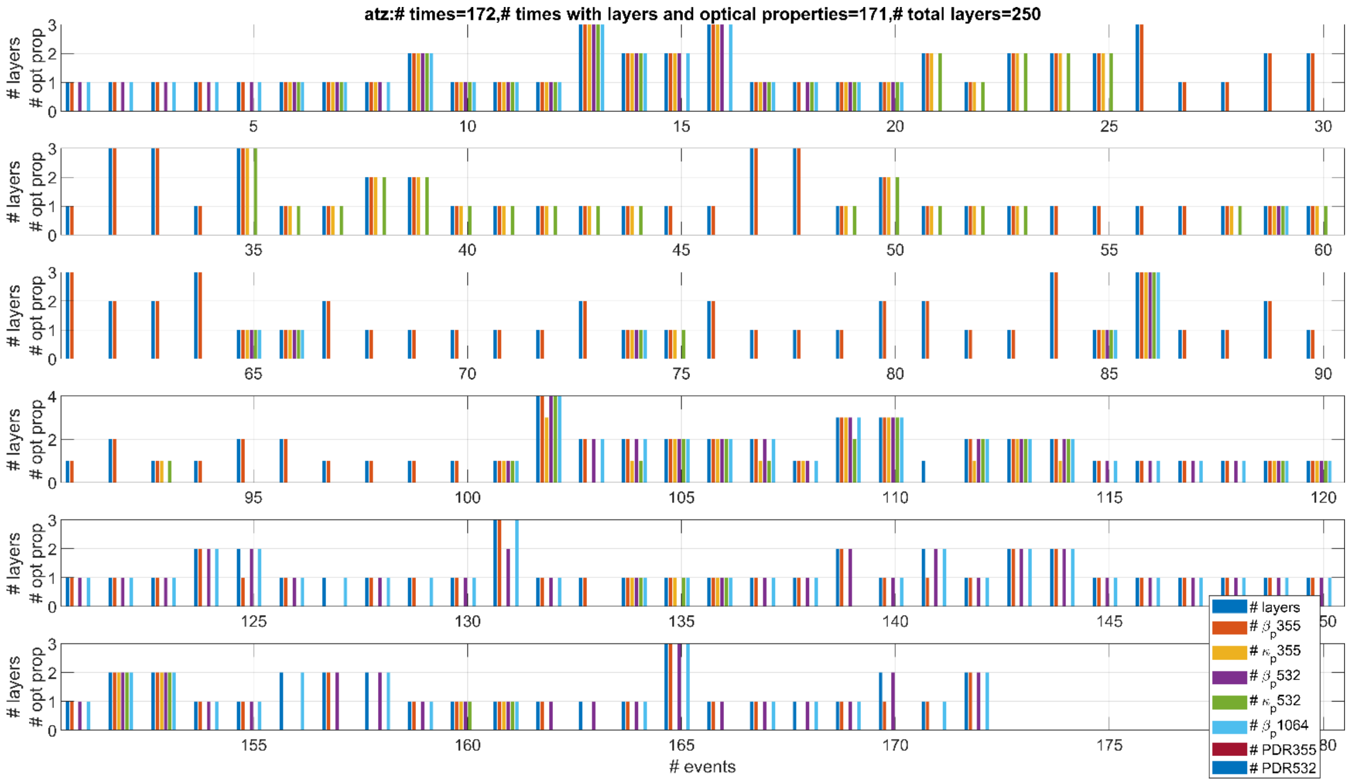

Figure S2. The number of times (events) when the layers were evaluated and the corresponding number of optical properties available in the layer. Example for the Athens station ("atz"). Layers have a biomass burning origin (fire source). For event 111 it was not feasible to determine any optical property.

S5 Intensive parameters in literature

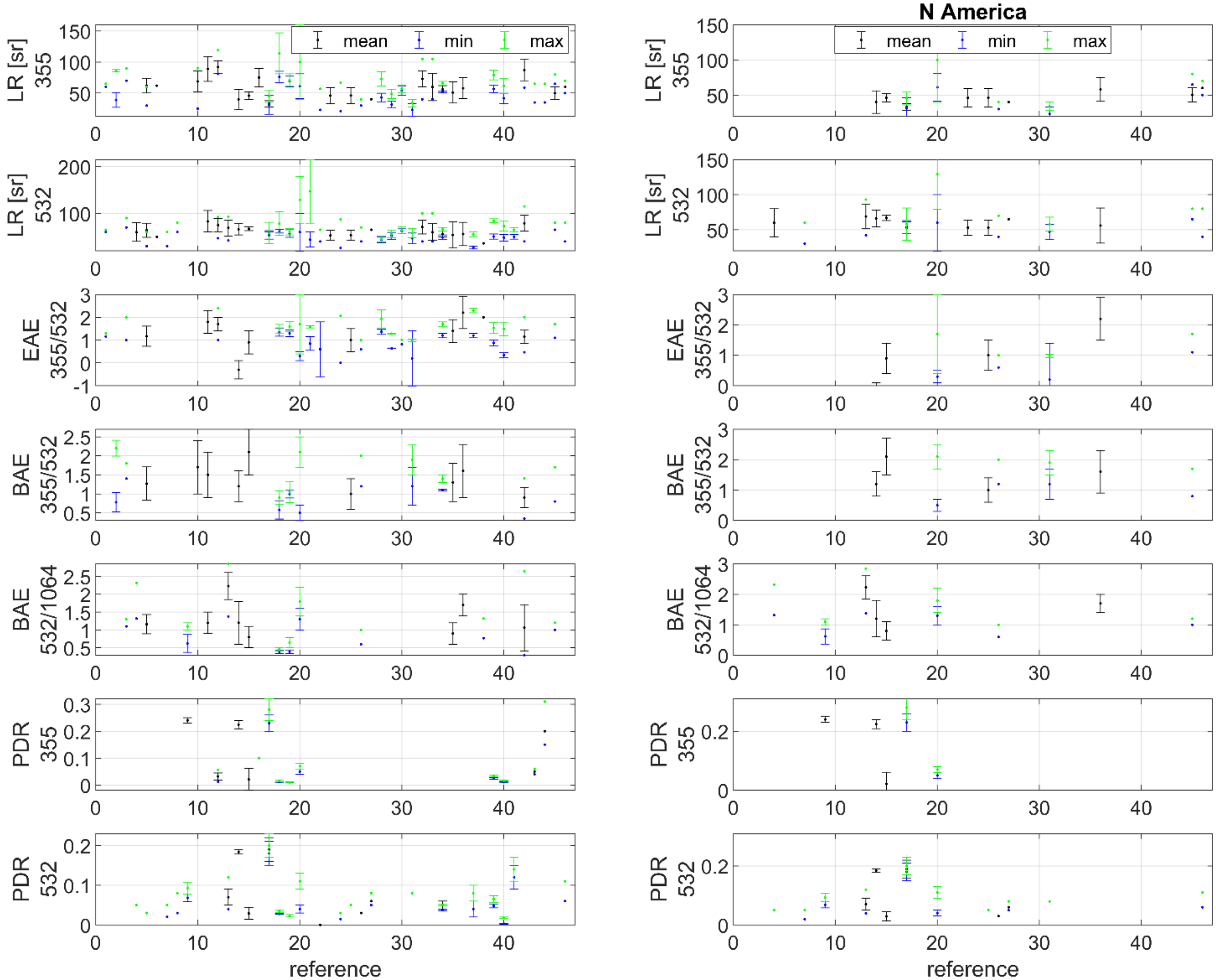

Figure S3. Intensive parameters for biomass burning, as reported in literature. The reference number corresponds to the references in Table S4.

Table S3. Values of the intensive parameters found in literature for biomass burning.

variable/ref		1	2	3	4	5	6	7	8	9	10	11	12	13	14	15	16	17	18	19	20	21	22	23
LR355	mean					62	62				69	89	92		40	46	75	33						46
	mear er					12					17	20	10		16	6	15	5						13
	min	60	39	70		30					25		81					31	76	69	61		23	
	min er		12															15	9	9	20			
	max	65	86	90		60					90		119					45	114	71	100		57	
	max er		2															9	33	10	60			
LR532	mean				60	64	50					83	75	69	66	67		53						53
	mear er				20	15						23	14	17	12	4		8						11
	min	60		70		30		30	60				47	42				54	62	57	60	44	40	
	min er																	9	4	8	40	16		
	max	65		90		60		60	80				92	93				58	78	61	129	147	65	
	max er																	23	25	7	50	68		
EAE	mean					1.17						1.8	1.7		-0.3	0.9								
	mear er					0.44						0.5	0.3		0.4	0.5								
	min	1.16		1									1						1.35	1.3	0.3	0.85	0.6	
	min er																		0.18	0.15	0.2	0.3		
	max	1.3		2									2.4						1.5	1.6	1.7	1.58	1.2	
	max er																		0.19	0.22	1.3	0.05		
BAE532/355	mean					1.27					1.7	1.5			1.2	2.1								
	mear er					0.44					0.7	0.6			0.4	0.6								
	min		0.78	1.4							0.9								0.58	0.99	0.5		1	
	min er		0.25																0.24	0.1	0.2			
	max		2.2	1.8							2.8								0.9	1.05	2.1		1.6	
	max er		0.21																0.18	0.28	0.4			
BAE1064/532	mean					1.16						1.2		2.23	1.2	0.8								
	mear er					0.27						0.3		0.38	0.6	0.3								
	min			1.1	1.32					0.62				1.38					0.39	0.39	1.3		1	
	min er									0.25									0.05	0.05	0.3			
	max			1.3	2.32					1.1				2.85					0.46	0.65	1.8		2.4	
	max er									0.1									0.05	0.14	0.4			
PDR355	mean									24			3.2		22.4	2.1		23						
	mear er									1			1.3		1.5	4		3						
	min												1.2					23	1.1	1	5			
	min er																	3	0.1	0.1	1			
	max												5.7				10	28	1.6	1	7			
	max er																	4	0.3	0.2	1			
PDR532	mean													7	18.4	2.9		19					0	
	mear er													2	0.6	1.5		3						
	min							2	3	6.8				4				18	2.8	2.3	4			
	min er									1								3	0.1	0.3	1			
	max				5	3		5	8	9.3				12				20	3.5	2.3	11			
	max er									1.5								3	0.3	0.3	2			
fresh (0)/aged(1)		0	1	0	1	1	1	0	1	1	1	1	1	1	1	1	0	1	0	1	1	1	1	1

variable/ref		24	25	26	27	28	29	30	31	32	33	34	35	36	37	38	39	40	41	42	43	44	45	46
LR355	mean		46		40					73	60	56	51	58						87			50	60
	mear er		13							13	22	6	17	17						17			10	
	min	21		30		42.9	31.7	54	23	40	40	52					56.5	41.6		59	35	35	65	50
	min er					6.8	5	7	10			1					5.7	8.3						
	max	67		40		73	48.8	57	34	105	105	66					79.2	61.7		130	65	65	80	70
	max er					11.6	7.7	6	6			3					7.9	12.3						
LR532	mean		53		65					71	60	56	54	56		36				79				40
	mear er		11							15	18	6	28	25						17				
	min	26		40		43.4	52.1	62	47	40	40	49			27		50.6	48.2	50	40			65	40
	min er					6.1	7.3	5	11			5			3		5.4	7.2	5					
	max	87		70		45.7	55.9	64	58	100	100	66			55		84.3	73.2	65	115			80	80
	max er					6.4	7.8	7	10			4			5		4.2	11	5					
EAE	mean		1										1.4	2.2		2				1.15				
	mear er		0.5										0.5	0.7						0.28				
	min	0		0.6		1.37	0.64	0.83	0.2			1.2			1.2		0.87	0.34		0.47			1.1	
	min er					0.12	0.01		1.2			0.1			0.1		0.13	0.1						
	max	1.3		1		1.93	1.28	1.02	0.98			1.7			2.3		1.54	1.49		2.01			1.7	
	max er					0.4	0.01		0.06			0.1			0.1		0.23	0.3						
BAE532/355	mean		1										1.3	1.6						0.9				
	mear er		0.4										0.5	0.7						0.26				
	min			1.2					1.2			1.1								0.35			0.8	
	min er								0.5			0.02												
	max			2					1.9			1.4								1.41			1.7	
	max er								0.4			0.1												
BAE1064/532	mean												0.9	1.7						1.06				
	mear er												0.3	0.3						0.65				
	min			0.6												0.77				0.29			1	
	min er																							
	max			1												1.32				2.65			1.2	
	max er																							
PDR355	mean																				5	20		
	mear er																							
	min																2.4	1.1			4	15		
	min er																0.3	0.1						
	max																3.4	1.6			6	31		
	max er																0.4	0.2						
PDR532	mean			3	6							5												
	mear er											1												
	min	1.5			5							3.8			4		4.8	0.3	12					6
	min er											0.2			2		0.5	0.1	3					
	max	3	5		8				8			5			8		6.5	1.8	14					11
	max er											0.2			2		0.8	0.2	3					
fresh (0)/aged(1)		1	1	1	1	0	1	1	1	0	1	1	0	1	1	0	0	1	0	1	1	1	0	1

Table S4. References for biomass burning intensive parameters

1. Alados-Arboledas, L., D. Müller, J. L. Guerrero-Rascado, F. Navas-Guzmán, D. Pérez-Ramírez, and F. J. Olmo, Optical and microphysical properties of fresh biomass burning aerosol retrieved by Raman lidar, and star-and sun-photometry, Geophys. Res. Lett., 38, L01807, doi:10.1029/2010GL045999, 2011.
2. Amiridis, V., D. S. Balis, E. Giannakaki, A. Stohl, S. Kazadzis, M. E. Koukouli, and P. Zanis, Optical characteristics of biomass burning aerosols over Southeastern Europe determined from UV-Raman lidar measurements, Atmos. Chem. Phys., 9, 2431–2440, 2009, www.atmos-chem-phys.net/9/2431/2009/.
3. Amiridis, V., C. Zerefos, S. Kazadzis, E. Gerasopoulos, K. Eleftheratos, M. Vrekoussis, A. Stohl, R.E. Mamouri, P. Kokkalis, A. Papayannis, K. Eleftheriadis, E. Diapouli, I. Keramitsoglou, C. Kontoes, V. Kotroni, K. Lagouvardos, E. Marinou, E. Giannakaki, E. Kostopoulou, C. Giannakopoulos, A. Richter, J.P. Burrows, N. Mihalopoulos, Impact of the 2009 Attica wild fires on the air quality in urban Athens, Atmos.Environ., 46, 536-544, doi:10.1016/j.atmosenv.2011.07.056, 2012.
4. Ancellet, G., J. Pelon, J. Totems, P. Chazette, A. Bazureau, M. Sicard, T. Di Iorio, F. Dulac, and M. Mallet, Long-range transport and mixing of aerosol sources during the 2013 North American biomass burning episode: analysis of multiple lidar observations in the western Mediterranean basin, Atmos. Chem. Phys., 16, 4725–4742, doi:10.5194/acp-16-4725-2016, 2016.
5. Baars, H., A. Ansmann, D. Althausen, R. Engelmann, B. Heese, D. Müller, P. Artaxo, M. Paixao, T. Pauliquevis, and R. Souza, Aerosol profiling with lidar in the Amazon Basin during the wet and dry season, J. Geophys. Res., 117, D21201, doi:10.1029/2012JD018338, 2012.
6. Balis, D. S., V. Amiridis, C. Zerefos, E. Gerasopoulos, M. Andreae, P. Zanis, A. Kazantzidis, S. Kazadzis, A. Papayannis, Raman lidar and sunphotometric measurements of aerosol optical properties over Thessaloniki, Greece during a biomass burning episode, Atmos. Environ., 37, 4529-4538, doi:10.1016/S1352-2310(03)00581-8, 2003.
7. Burton, S. P., R. A. Ferrare, C. A. Hostetler, J. W. Hair, R. R. Rogers, M. D. Obland, C. F. Butler, A. L. Cook, D. B. Harper, and K. D. Froyd, Aerosol classification using airborne High Spectral Resolution Lidar measurements – methodology and examples, Atmos. Meas. Tech., 5, 73–98, doi:10.5194/amt-5-73-2012, 2012.
8. Burton, S. P., R. A. Ferrare, C. A. Hostetler, J. W. Hair, R. R. Rogers, M. D. Obland, C. F. Butler, A. L. Cook, D. B. Harper, and K. D. Froyd, Aerosol classification using airborne High Spectral Resolution Lidar measurements – methodology and examples, Atmos. Meas. Tech., 5, 73–98, doi:10.5194/amt-5-73-2012, 2012.
9. Burton, S. P., J. W. Hair, M. Kahnert, R. A. Ferrare, C. A. Hostetler, A. L. Cook, D. B. Harper, T. A. Berkoff, S. T. Seaman, J. E. Collins, M. A. Fenn, and R. R. Rogers, Observations of the spectral dependence of linear particle depolarization ratio of aerosols using NASA Langley airborne High Spectral Resolution Lidar, Atmos. Chem. Phys., 15, 13453–13473, doi:10.5194/acp-15-13453-2015, 2015.

10. Giannakaki, E., D. S. Balis, V. Amiridis, and C. Zerefos, Optical properties of different aerosol types: seven years of combined Raman-elastic backscatter lidar measurements in Thessaloniki, Greece, Atmos. Meas. Tech., 3, 569–578, doi:10.5194/amt-3-569-2010, 2010.
11. Giannakaki, E., A. Pfüller, K. Korhonen, T. Mielonen, L. Laakso, V. Vakkari, H. Baars, R. Engelmann, J. P. Beukes, P. G. Van Zyl, M. Josipovic, P. Tiitta, K. Chiloane, S. Piketh, H. Lihavainen, K. E. J. Lehtinen, and M. Komppula, One year of Raman lidar observations of free-tropospheric aerosol layers over South Africa, Atmos. Chem. Phys., 15, 5429–5442, doi:10.5194/acp-15-5429-2015, 2015.
12. Giannakaki, E., P. G. van Zyl, D. Müller, D. Balis, and M. Komppula, Optical and microphysical characterization of aerosol layers over South Africa by means of multi-wavelength depolarization and Raman lidar measurements, Atmos. Chem. Phys., 16, 8109–8123, doi:10.5194/acp-16-8109-2016, 2016.
13. Groß, S., M. Esselborn, B. Weinzierl, M. Wirth, A. Fix, and A. Petzold, Aerosol classification by airborne high spectral resolution lidar Observations, Atmos. Chem. Phys., 13, 2487–2505, doi:10.5194/acp-13-2487-2013, 2013.
14. Haarig, M., Ansmann, A., Baars, H., Jimenez, C., Veselovskii, I., Engelmann, R., and Althausen, D.: Depolarization and lidar ratios at 355, 532, and 1064 nm and microphysical properties of aged tropospheric and stratospheric Canadian wildfire smoke, Atmos. Chem. Phys., 18, 11847-11861, https://doi.org/10.5194/acp-18-11847-2018, 2018.
15. Haarig, M., Ansmann, A., Baars, H., Jimenez, C., Veselovskii, I., Engelmann, R., and Althausen, D.: Depolarization and lidar ratios at 355, 532, and 1064 nm and microphysical properties of aged tropospheric and stratospheric Canadian wildfire smoke, Atmos. Chem. Phys., 18, 11847-11861, https://doi.org/10.5194/acp-18-11847-2018, 2018.
16. Heese, B., and M. Wiegner, Vertical aerosol profiles from Raman polarization lidar observations during the dry season AMMA field campaign, J. Geophys. Res., 113, D00C11, doi:10.1029/2007JD009487, 2008.
17. Hu, Q., Goloub, P., Veselovskii, I., Bravo-Aranda, J.-A., Popovici, I., Podvin, T., Haeffelin, M., Lopatin, A., Pietras, C., Huang, X., Torres, B., and Chen, C.: A study of long-range transported smoke aerosols in the Upper Troposphere/Lower Stratosphere, Atmos. Chem. Phys., 19, 1173–1193, https://doi.org/10.5194/acp-19-1173-2019, 2019.
18. Janicka, L., I. S. Stachlewska, Properties of biomass burning aerosol mixtures derived at fine temporal and spatial scales from Raman lidar measurements: Part I optical properties, Atmos. Chem. Phys. Discuss., https://doi.org/10.5194/acp-2019-207, 2019.
19. Janicka, L., I. S. Stachlewska, Properties of biomass burning aerosol mixtures derived at fine temporal and spatial scales from Raman lidar measurements: Part I optical properties, Atmos. Chem. Phys. Discuss., https://doi.org/10.5194/acp-2019-207, 2019.
20. Janicka, L., I. S. Stachlewska, I. Veselovskii, H. Baars, Temporal variations in optical and microphysical properties of mineral dust and biomass burning aerosol derived from daytime Raman lidar observations over Warsaw, Poland, Atmos. Environ., 169, 162-174, http://dx.doi.org/10.1016/j.atmosenv.2017.09.022, 2017.

21. Mariano, G.L., F.J.S. Lopes, M.P.P.M. Jorge, E. Landulfo, Assessment of biomass burnings activity with the synergy of sunphotometric and LIDAR measurements in São Paulo, Brazil, Atmos. Res., 98, 486-499, doi:10.1016/j.atmosres.2010.08.025, 2010.
22. Mattis, I., A. Ansmann, U. Wandinger, and D. Müller, Unexpectedly high aerosol load in the free troposphere over central Europe in spring//summer 2003, G.R.L., 30, 2178, doi:10.1029/2003GL018442, 2003.
23. Mattis, I., D. Mu¨ller, A. Ansmann, U. Wandinger, J. Preißler, P. Seifert, and M. Tesche, Ten years of multiwavelength Raman lidar observations of free-tropospheric aerosol layers over central Europe: Geometrical properties and annual cycle, J. Geophys. Res., 113, D20202, doi:10.1029/2007JD009636, 2008.
24. Müller, D., I. Mattis, U. Wandinger, A. Ansmann, D. Althausen, and A. Stohl, Raman lidar observations of aged Siberian and Canadian forest fire smoke in the free troposphere over Germany in 2003: Microphysical particle characterization, J. Geophys. Res., 110, D17201, doi:10.1029/2004JD005756, 2005.
25. Müller, D., A. Ansmann, I. Mattis, M. Tesche, U. Wandinger, D. Althausen, and G. Pisani, Aerosol-type-dependent lidar ratios observed with Raman lidar, J. Geophys. Res., 112, D16202, doi:10.1029/2006JD008292, 2007.
26. Müller, D., A. Kolgotin, I. Mattis, A. Petzold, and A. Stohl, Vertical profiles of microphysical particle properties derived from inversion with two-dimensional regularization of multiwavelength Raman lidar data: experiment, Appl. Opt., 50, 2069-2079, 2011.
27. Murayama, T., D. Müller, K. Wada, A. Shimizu, M. Sekiguchi, and T. Tsukamoto, Characterization of Asian dust and Siberian smoke with multiwavelength Raman lidar over Tokyo, Japan in spring 2003, Geophys. Res. Lett., 31, L23103, doi:10.1029/2004GL021105, 2004.
28. Nicolae, D., A. Nemuc, D. Müller, C. Talianu, J. Vasilescu, L. Belegante, and A. Kolgotin, Characterization of fresh and aged biomass burning events using multiwavelength Raman lidar and mass spectrometry, J. Geophys. Res. Atmos., 118, 2956–2965, doi:10.1002/jgrd.50324, 2013.
29. Nicolae, D., A. Nemuc, D. Müller, C. Talianu, J. Vasilescu, L. Belegante, and A. Kolgotin, Characterization of fresh and aged biomass burning events using multiwavelength Raman lidar and mass spectrometry, J. Geophys. Res. Atmos., 118, 2956–2965, doi:10.1002/jgrd.50324, 2013.
30. Noh, Y. M., D. Müller, D. H. Shin, H. Lee, J. S. Jung, K. H. Lee, M. Cribb, Z. Li, Y. J. Kim, Optical and microphysical properties of severe haze and smoke aerosol measured by integrated remote sensing techniques in Gwangju, Korea, Atmos. Environ., 879–888, doi:10.1016/j.atmosenv.2008.10.058, 2009.
31. Ortiz-Amezcua, P., J. L. Guerrero-Rascado, M. J. Granados-Muñoz, J. A. Benavent-Oltra, C. Böckmann4, S. Samaras, I. S. Stachlewska, Ł. Janicka, H. Baars, S. Bohlmann, and L. Alados-Arboledas, Microphysical characterization of long-range transported biomass burning particles from North America at three EARLINET stations, Atmos. Chem. Phys., 17, 5931–5946, doi:10.5194/acp-17-5931-2017, 2017.

32. Mylonaki, M., A. Papayannis, R. Mamouri, A. Argyrouli, P. Kokkalis, G. Tsaknakis and O. Soupiona, Aerosol optical properties variability during biomass burning events observed by the EOLE-AIAS depolarization lidars over Athens, Greece (2007-2016), 28th ILRC, Bucharest, Romania (2017).
33. Mylonaki, M., A. Papayannis, R. Mamouri, A. Argyrouli, P. Kokkalis, G. Tsaknakis and O. Soupiona, Aerosol optical properties variability during biomass burning events observed by the EOLE-AIAS depolarization lidars over Athens, Greece (2007-2016), 28th ILRC, Bucharest, Romania (2017).
34. Nepomuceno Pereira, S., J. Preißler, J. L. Guerrero-Rascado, A. M. Silva, and F. Wagner, Forest Fire Smoke Layers Observed in the Free Troposphere over Portugal with a Multiwavelength Raman Lidar: Optical and Microphysical Properties, Scienttific World, Journal, 2014, Article ID 421838, 11 pages, http://dx.doi.org/10.1155/2014/421838. 2014.
35. Preißler, J., F. Wagner, J. L. Guerrero-Rascado, and A. M. Silva, Two years of free-tropospheric aerosol layers observed over Portugal by lidar, J. GEOPHYS. RES., 118, 3676–3686, doi:10.1002/jgrd.50350, 2013.
36. Preißler, J., F. Wagner, J. L. Guerrero-Rascado, and A. M. Silva, Two years of free-tropospheric aerosol layers observed over Portugal by lidar, J. GEOPHYS. RES., 118, 3676–3686, doi:10.1002/jgrd.50350, 2013.
37. Samaras, S., D. Nicolae, C. Böckmann, J. Vasilescu, I. Binietoglou, L. Labzovskii, F. Toanca, A. Papayannis, Using Raman-lidar-based regularized microphysical retrievals and Aerosol Mass Spectrometer measurements for the characterization of biomass burning aerosols, Journal of Computational Physics 299, 156–174, http://dx.doi.org/10.1016/j.jcp.2015.0, 2015.
38. Sicard, M., M Mallet, D. Garc´ıa-Vizca´ıno, A Comer´on, F Rocadenbosch, P Dubuisson and C Mu˜noz-Porcar, Intense dust and extremely fresh biomass burning outbreak in Barcelona, Spain: characterization of their optical properties and estimation of their direct radiative forcing, Environ. Res. Lett. 7, 034016 (6pp), doi:10.1088/1748-9326/7/3/034016, 2012.
39. Stachlewska, I. S., O. Zawadzka and R. Engelmann, Effect of HeatWave Conditions on Aerosol Optical Properties Derived from Satellite and Ground-Based Remote Sensing over Poland, Remote Sens., 9, 1199; doi:10.3390/rs9111199, 2017.
40. Stachlewska, I. S., M. Samson, O. Zawadzka , K. M. Harenda, L. Janicka, P. Poczta, D. Szczepanik, B. Heese, D. Wang, K. Borek, E. Tetoni, E. Proestakis, N. Siomos, A. Nemuc, B. H. Chojnicki, K. M. Markowicz, A. Pietruczuk, A. Szkop, D. Althausen, k. Stebel , D. Schuettemeyer and C. Zehner, Modification of Local Urban Aerosol Properties by Long-Range Transport of Biomass Burning Aerosol, Remote Sens., 10, 412; doi:10.3390/rs10030412, 2018.
41. Sugimoto, N., B. Tatarov, A. Shimizu, I. Matsui, and T. Nishizawa, Optical Characteristics of Forest-Fire Smoke Observed with Two-Wavelength Mie-Scattering Lidars and a High-Spectral-Resolution Lidar over Japan, SOLA, 6, 093−096, doi:10.2151/sola.2010-024, 2010.

42. Tesche, M., D. Müller, S. Gross, A. Ansmann, D. Althausen, V. Freudenthaler, B. Weinzierl, A. Veira and A. Petzold, Optical and microphysical properties of smoke over Cape Verde inferred from multiwavelength lidar measurements, Tellus, 63B, 677–694, DOI: 10.1111/j.1600-0889.2011.00549.x, 2011.

43. Vaughan, g., A. P. Draude, H. M. A. Ricketts, D. M. Schultz, M. Adam, J. Sugier, and D. P. Wareing, Transport of Canadian forest fire smoke over the UK as observed by lidar, Atmos. Chem. Phys., 18, 11375–11388, https://doi.org/10.5194/acp-18-11375-2018, 2018.

44. Vaughan, G., A. P. Draude, H. M. A. Ricketts, D. M. Schultz, M. Adam, J. Sugier, and D. P. Wareing, Transport of Canadian forest fire smoke over the UK as observed by lidar, Atmos. Chem. Phys., 18, 11375–11388, https://doi.org/10.5194/acp-18-11375-2018, 2018.

45. Veselovskii, I, D. N Whiteman, M. Korenskiy, A. Suvorina, A. Kolgotin, A. Lyapustin, Y. Wang, M. Chin, H. Bian, T. L. Kucsera, D. Pérez-Ramírez, and B. Holben, Characterization of forest fire smoke event near Washington, DC in summer 2013 with multi-wavelength lidar, Atmos. Chem. Phys., 15, 1647–1660, doi:10.5194/acp-15-1647-2015, 2015.

46. Wandinger, U., D. Müller, C. Bo¨ckmann, D. Althausen, V. Matthias, J. Bo¨senberg, V. Weiß, M. Fiebig, M. Wendisch, A. Stohl, and A. Ansmann, Optical and microphysical characterization of biomassburning and industrial-pollution aerosols from multiwavelength lidar and aircraft measurements, J. Geophys. Res., 107, NO. D21, 8125, doi:10.1029/2000JD000202, 2002.

S6 Example number of layers selected and corresponding intensive optical parameters available for each layer

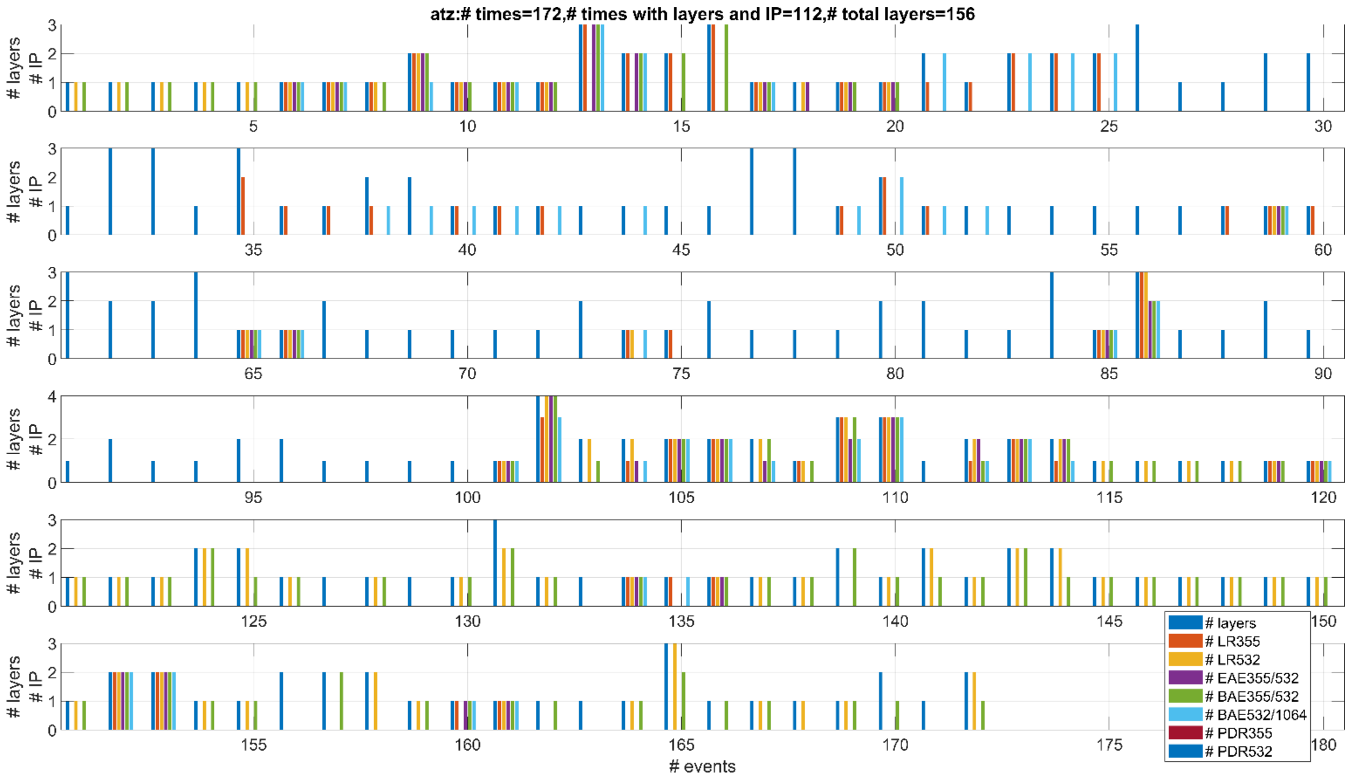

Figure S4. The number of times (events) when the layers were evaluated and the corresponding number of intensive parameters available in the layer. Example for Athens station ("atz"). Layers have a biomass burning origin (fire source).